Linear Stratospheric Gravity Waves above Convective Thermal Forcing

RAJUL E. PANDYA

National Center for Atmospheric Research, Boulder, Colorado*

M. JOAN ALEXANDER+

Department of Atmospheric Sciences, University of Washington, Seattle, Washington

(Manuscript received 15 April 1998, in final form 15 October 1998)

ABSTRACT

The spectra of linear gravity waves generated by a time-varying tropospheric thermal forcing representing organized convection are compared to the spectra of stratospheric gravity waves generated by organized convection in a fully nonlinear two-dimensional squall line simulation. The resemblance between the spectra in the two simulations suggests that stratospheric gravity waves above convection can be understood primarily in terms of the linear response to a time- and space-dependent thermal forcing. In particular, the linear response to thermal forcing accounts for the correlation between the dominant vertical wavelength of the stratospheric waves and the depth of the tropospheric convection as well as the the fact that the dominant frequency of the stratospheric waves is the same as the frequency of oscillation of the main convective updraft.

1. Introduction

Atmospheric waves play a crucial role in the dynamics of the middle atmosphere (Andrews et al. 1987). Wind perturbations associated with atmospheric waves dominate the observational variability, and the momentum transported by waves shapes the observed pattern of the mean zonal wind (Gage and Balsley 1984). Thus, understanding wave sources and their generation mechanisms is crucial to successfully modeling the general circulation of the atmosphere.

Convective heating has been appreciated as an important source for planetary-scale waves since Holton (1973) demonstrated that a response very similar to observed Kelvin waves in the tropical stratosphere can arise from stochastically distributed heat sources in a linear model with realistic zonal wind variations. Salby and Garcia (1987) showed that the large-scale, near-field, vertical wavenumber response to a heat source is primarily sensitive to only the depth of the heating and is only weakly sensitive to the detailed vertical profile of the heating. Thus many features of the observations of convectively forced planetary-scale waves can be accounted for within a linear framework using only the depth of the convective heating and the zonal mean wind variations.

A similar approach has been applied to smaller-scale waves in the inertia-gravity wave portion of the spectrum (Manzini and Hamilton 1993; Bergman and Salby 1994). Manzini and Hamilton (1993) examined the role of convective heating in forcing waves in the stratosphere of the SKYHI general circulation model (GCM). Their analysis included both planetary-scale as well as large-scale inertia–gravity waves with zonal wavenumbers less than 25. They found that the latent heating in convection was an important wave-forcing mechanism in SKYHI globally, and that the convective forcing was in fact responsible for most of the Eliassen–Palm (EP) flux (Edmon et al. 1980) in the Tropics. Manzini and Hamilton (1993) further compared the waves found in the full GCM simulation to those forced by heating (prescribed from the GCM) in a linear model. The linear model reproduced many of the details in the wave field seen in the full GCM, but with somewhat larger wave amplitudes. This important comparison lends credence to the types of linear analyses described above and to the Garcia and Salby (1987) analysis of the far-field response to prescribed heating.

Bergman and Salby (1994) derived a space- and time-variable heating function based on 4-hourly global cloud imagery data at 0.5° resolution. They used maps of the

* The National Center for Atmospheric Research is sponsored by the National Science Foundation.

+ Current affiliation: Colorado Research Associates, Boulder, Colorado.

Corresponding author address: Rajul Pandya, NCAR, P.O. Box 3000, Boulder, CO 80307-3000.
E-mail: pandya@ncar.ucar.edu

cold cloud tops to describe the heating $Q(\lambda, \theta, \zeta, t)$ (as a function of longitude, latitude, altitude, and time, respectively) for input to a linear model. Their results applied to planetary-scale waves as well as the inertia-gravity wave end of the gravity wave spectrum, but by extrapolating to higher frequencies, they estimated that gravity waves carry 60% of the EP flux of waves forced by convection in the Tropics. However, application of this linear forcing mechanism has not been tested for waves with mesoscale wavelengths and higher frequencies.

Alexander et al. (1995, hereafter AHD) studied convectively forced gravity waves in a two-dimensional simulation of organized convection. Spectral analysis of the mesoscale, high-frequency gravity waves in the stratosphere above the simulated storm showed a strong correlation between the vertical wavelengths of the gravity waves and the depth of the convective heating, in agreement with Salby and Garcia's (1987) analysis. This result suggested that prescribed heating in a linear model might also characterize convectively generated gravity waves at these smaller scales and higher frequencies. AHD also found that the periodicity of the tropospheric convection determined the frequency of the stratospheric gravity waves via the mechanical oscillator mechanism of Fovell et al. (1992), and that their eastward-moving storm preferentially excited westward-propagating waves. Fovell et al. (1992) noted that the gravity waves that are preferentially excited are those propagating opposite the direction of the storm and attributed the preferential generation of rearward-propagating waves to the rearward storm-relative motion of updraft ''cells'' (periodic or quasiperiodic regions of active convection). It is interesting to note that Yang and Houze (1995) suggested that these tropospheric cells are themselves associated with gravity waves.

Global patterns in latent heating are observable in data from the recent Tropical Rainfall Measurement Mission (Simpson et al. 1996); if direct connections between latent heating and the stratospheric waves can be derived, then these data could, in principal, be used to specify wave sources in GCMs. Our analysis in this paper follows the analysis of Manzini and Hamilton (1993) but here we use a mesoscale convection simulation rather than a GCM. In that spirit, we test the idea of using prescribed heating in a linear model by comparing the waves generated in such a model to the waves generated in a fully nonlinear model with microphysics. Our results show that knowledge of the space- and time-variable latent heating function $Q(x, z, t)$ in a linear model can be used to qualitatively characterize the convectively generated vertical wavelength and frequency spectra, although the amplitudes of the spectra are larger than that predicted from a full nonlinear model with microphysics. Nonlinear processes reduce the amplitudes of waves with a horizontal wavelength of less than 100 km. The nonlinear effects are spread evenly across vertical wavelengths and frequencies and so have no important influence on determining the dominant peaks in the frequency and vertical wavelength spectra. The defining spectral characteristics are instead related directly to the depth and time variability of the thermal forcing.

2. Quasi-linear simulation

In this section, we compare waves in a nonlinear squall line simulation to the waves in a ''dry quasi-linear'' simulation. The nonlinear simulation is the two-dimensional squall line simulation with parameterized microphysics described in AHD. In the dry quasi-linear simulation, the microphysical processes are turned off and all motions are instead generated by a time- and space-varying pattern of thermal forcing. To ensure that this thermal forcing represents real convection, we use the pattern of latent heating and cooling from the nonlinear simulation of AHD. We divided the heating and cooling pattern by 1000 in order to limit the amplitude of the resulting waves and approximate linear dynamics. For this reason, we refer to this simulation as quasi-linear.

The environmental winds and thermodynamic profile of the nonlinear and quasi-linear simulations were identical, and the initial conditions are shown in Fig. 1 of AHD (the initial conditions are reproduced in Fig 7). The numerical model and details of the integration are also identical in the two simulations; these are discussed in section 2 of AHD. The horizontal grid spacing is 1.5 km and vertical grid spacing in the stratosphere varies from 280 to 119 m, decreasing with height. Two types of dissipation mechanisms can act in this model: 1) a fourth-order hyperdiffusion that effectively damps perturbations with horizontal scales less than 10 km and 2) a Richardson number–dependent mixing parameterization. The mixing in these model simulations is only active inside the convective cloud in the nonlinear squall line simulation. There is no background shear in the stratosphere and wave amplitudes do not grow large enough within the 32-km domain depth to become unstable even in the nonlinear simulation.

The pattern of latent heating and cooling in the nonlinear squall line simulation was sampled every 120 s and used to update the time- and space-varying pattern of forcing in the quasi-linear simulation. Values of the forcing at times not divisible by 120 s were computed by linear interpolation. Sampling the instantaneous pattern of heating and cooling at 120 s limits the period of the forcing in the quasi-linear simulation to $\tau > 240$ s. Waves we are interested in, however, have significantly longer periods than 240 s, so the time resolution of the forcing should be sufficient to generate all the stratospheric waves of interest.

Figure 1a shows the scaled vertical velocity field at time 6 h generated by the time- and space-varying pat-

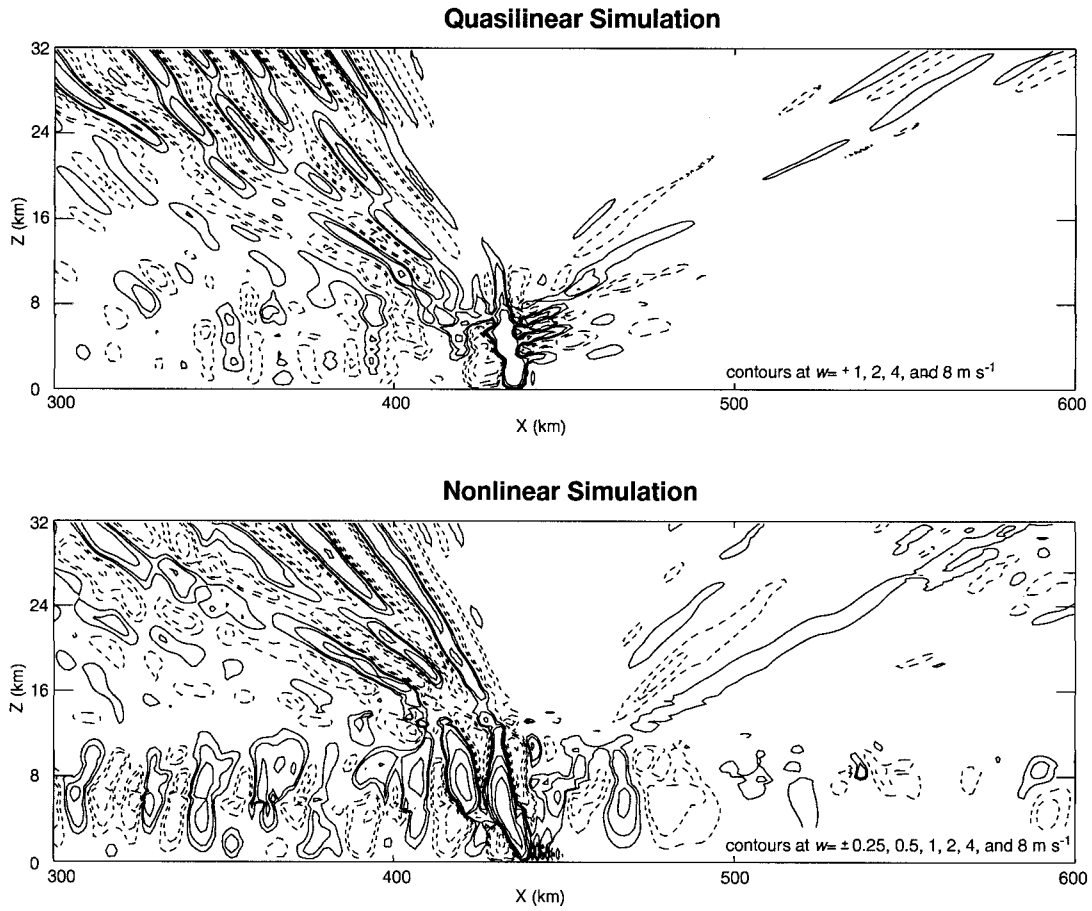

FIG. 1. (a) Scaled vertical velocity (contours shown are ± 1, 2, 4, and 8 m s^{-1}; negative contours dashed) 6 h into the quasi-linear simulation; (b) vertical velocity (contours shown are ± 0.25, 0.5, 1, 2, 4, and 8 m s^{-1}; negative contours dashed) 6 h into the nonlinear squall line simulation.

tern of thermal forcing in the quasi-linear simulation. In order to facilitate the comparison of the quasi-linear and nonlinear simulations, the vertical velocity field in the quasi-linear simulation was multiplied by 1000, the same factor the heating was divided by, before being plotted. In the troposphere, the strongest updraft occurs at ~450 km and a number of weaker updrafts occur to the west of the main updraft. The updrafts tend to alternate with downdrafts; this structure resembles the vertical velocity cells visible in the nonlinear simulation of AHD, which is shown in Fig. 1b for easy comparison. (Care should be taken in comparing Figs. 1a and 1b since the contours are not the same in the two figures.) Note that the storm in Fig. 1b propagates eastward but the domain translates eastward to follow it so that the convective line remains near the center of the domain. In the quasi-linear simulation the peak heating remains centered in the domain. In both cases this is equivalent to viewing the stratospheric waves from the reference frame of the upper-tropospheric winds. Although it is difficult to tell from Fig. 1, the amplitudes of the oscillations in the troposphere in the quasi-linear and nonlinear cases are similar, although the detailed circulations are considerably different. Pandya and Durran (1996) also found that the tropospheric linear gravity wave response to a specified thermal forcing did not reproduce the detailed mesoscale features of the tropospheric circulation of real squall lines.

In the stratosphere, the vertical velocity contours in Fig. 1a slant away from the region of the thermal forcing, consistent with gravity waves transporting energy outward and upward from the regions of the main tropospheric updraft and the cell-like velocity features that trail it. In both simulations, the stratospheric wave field after 4 h is dominated by waves to the west of the main tropospheric updraft; our analysis will focus on these waves. As mentioned in the introduction, Fovell et al. (1992) related the dominance of westward-propagating waves in the stratosphere to the storm's eastward propagation. The dominant slope of the vertical velocity contours in the stratospheres of the two simulations are similar, although the nonlinear simulation shows a slightly more fanlike character to the waves. The vertical velocity field in the quasi-linear simulation also has

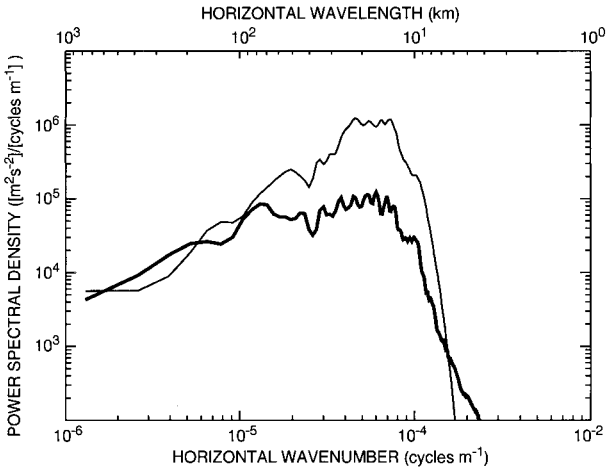

FIG. 2. Power spectra of the stratospheric vertical velocity as a function of horizontal wavenumber for the quasi-linear (thin line) and nonlinear (thick line) simulations.

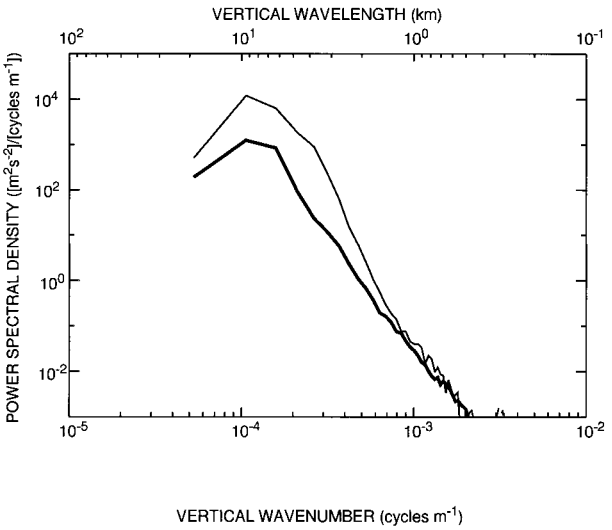

FIG. 3. Power spectra of the stratospheric vertical velocity as a function of vertical wavenumber for the quasi-linear (thin line) and nonlinear (thick line) simulations.

higher amplitude than the vertical velocity field in the nonlinear simulation. Nevertheless, the overall similarity of the upper-level vertical velocity field in the nonlinear and linear simulations suggests that the qualitative character of the stratospheric gravity waves above convection can be explained in terms of the linear response of a stably stratified fluid to a time- and space-varying thermal forcing.

3. Comparison of nonlinear and quasi-linear spectra

Even though the waves in Fig. 1a are approximately linear, the vertical velocity field is quite complex. A spectral analysis of the vertical velocity field was performed in order to gain insight into the nature of the gravity waves that make up the stratospheric response to the tropospheric heating. Because most of the wave activity in the stratosphere is in westward-propagating waves, our analysis will be restricted to westward-propagating waves.

The spectral analysis utilizes the discrete fast Fourier transform to transform from (x, t) to (k, ω), where k is the horizontal wavenumber and ω is the frequency. This is done at each vertical level between 12 and 32 km. The transform is applied to the entire 840 km wide domain. Power spectral density (PSD) is computed via the periodogram estimate (Percival and Walden 1993), which is assumed to be one-sided in k and two-sided in ω, that is,

$$\mathrm{PSD}(k, \omega) = 2\frac{\Delta x \Delta t}{N_x N_t}|\mathrm{FFT}(k > 0, \omega)|^2,$$

where Δx and Δt are the horizontal and time resolution, respectively; and N_x and N_t are the number of points in space and time. One-dimensional spectra for westward-propagating waves in k and ω are computed by integrating over k and $\omega > 0$, respectively. To compute the vertical wavenumber (m) spectra, the dispersion relation is used to relate PSD(k, ω) to PSD(m), and then the PSD(m) are binned. In a compressible atmosphere the decrease of density ρ with height leads to the growth in the vertical velocity amplitudes of the waves proportional to $\rho^{-1/2}$. Before averaging the spectra at different altitudes, the spectra are scaled with height accordingly. The spectral amplitudes shown are representative of an altitude of 13 km, which is just above the tropopause. In the quasi-linear case, the vertical velocity was multiplied by 1000 before the power spectra were computed. This scaling was meant to compensate for the factor of 1000 divided from the thermal forcing.

Figure 2 shows the power spectral density as a function of horizontal wavenumber in the quasi-linear (thin line) and nonlinear (thick line) simulation. The two agree for horizontal wavelengths greater than 100 km, but the quasi-linear spectrum has significantly more power than the nonlinear spectrum in modes with horizontal wavelengths less than 100 km. Recall from the discussion of Fig. 1 that the vertical velocity field in the quasi-linear simulation showed considerably more amplitude than the nonlinear simulation. The results of the horizontal spectra suggest that the differences are the result of too much energy in the short horizontal wavelength modes in the quasi-linear simulation; nonlinear effects seem to have an impact on stratospheric waves with horizontal wavelengths less than 100 km.

Vertical wavenumber spectra are shown in Fig. 3. The spectrum in the quasi-linear simulation (thin line) resembles the spectrum in the nonlinear simulation (thick line) qualitatively; both show a broad peak at vertical wavelengths near 8 km. Quantitatively, however, the quasi-linear spectrum has a much larger amplitude than

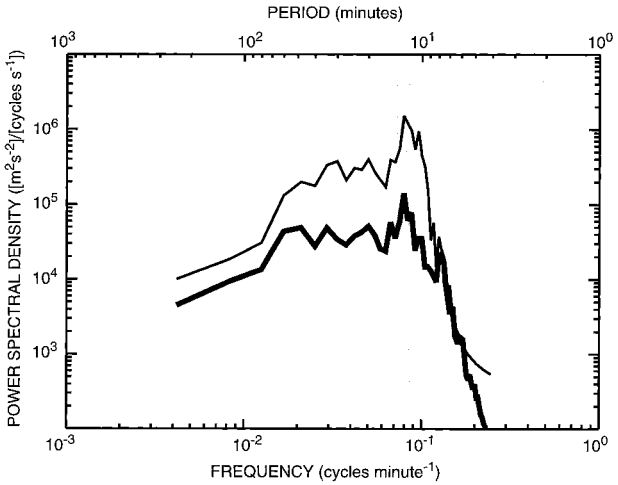

FIG. 4. Power spectra of the stratospheric vertical velocity as a function of frequency for the quasi-linear (thin line) and linear (thick line) simulations. The gray bar marks the dominant period of 12 min.

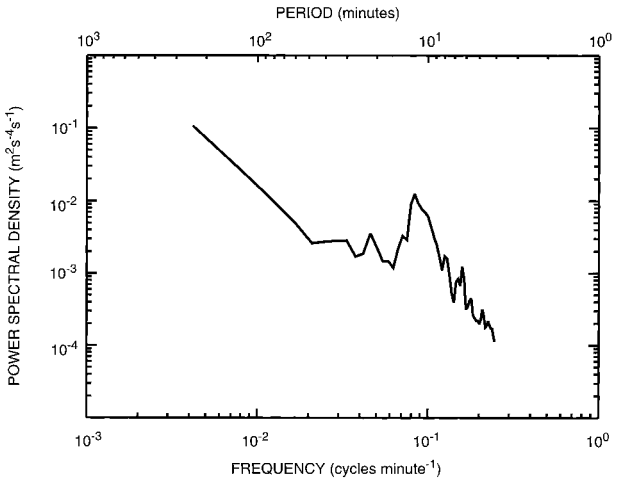

FIG. 5. Power spectrum of the thermal forcing as a function of frequency.

the nonlinear spectrum at all vertical wavelengths. Nevertheless, the ability of the quasi-linear simulation to reproduce the spectral peak near ~8 km suggests that nonlinear effects are not important in modifying the location of the spectral peak.

AHD related the spectral peak at vertical wavelengths of 6–10 km to the depth of the convective thermal forcing in the troposphere. The thermal forcing in the quasi-linear model includes a deep region of heating that resembles the positive half of a sine wave with a vertical wavelength of ~16 km (i.e., heating extended from 0–8 km with a peak at ~4 km). Numerous linear studies have demonstrated that a half-sine heating excites gravity waves with vertical wavelengths of twice the depth of the heating (Lin and Smith 1986; Bretherton 1988; Nicholls et al. 1991; Pandya et al. 1993; Mapes 1993). The change in the buoyancy by a factor of ~2 at the tropopause suggests that the vertical wavelength in the stratosphere would be one-half that of the waves in the troposphere due to refraction. Thus, the heating depth of 8 km corresponds to vertical wavelengths of 8 km in the stratosphere. There are a few observations that suggest a correlation between the deep convection and long vertical wavelength stratospheric gravity waves (Larsen et al. 1982; Sato 1993; Dewan et al. 1998). For larger-scale waves, Salby and Garcia (1987) also found a similar dependence of the vertical wavelength on the depth of the thermal forcing.

Figure 4 compares the frequency spectra in the quasi-linear (thin line) and nonlinear (thick line) simulations. Qualitatively, the spectra resemble one another closely; both show a spectral peak at a period of ~12 min and a relatively flat spectrum at longer periods out to approximately 1 h. From the dispersion relation for gravity waves, $\omega = N\cos\phi$, where ϕ is the angle of the phase lines measured from the vertical (Holton 1992), and the spectral peak at ~12 min corresponds to stratospheric gravity waves with phase lines at an angle of 64° from the vertical; this is visible in the vertical velocity field in both the quasi-linear and nonlinear simulation. The longer period waves in the frequency spectra apparently create the fanlike distribution of the phase lines to the west of the main 64° signal.

AHD attributed the PSD peak near 12 min to the mechanical oscillator mechanism (Fovell et al. 1992), in which stratospheric gravity waves are forced mechanically by the vertical motion and pressure perturbations in the troposphere. In the nonlinear simulation, the vertical velocity periodicity is tied to the production of cells in the convectively active part of the system. These cells produce and evaporate rain and therefore release and absorb heat. The power spectrum of the latent heat released and absorbed by the cells in the nonlinear model is shown in Fig. 5 and has a peak at ~12 min. Applying this thermal forcing in the quasi-linear simulation produces stratospheric frequency spectrum with a peak at ~12 min. These results indicate that in real storms the cellularity of the convection determines the frequencies of the dominant stratospheric waves via the linear response of the atmosphere to the frequencies of the convectively generated thermal forcing.

4. The linear model

In spite of the simplification of the quasi-linear model, it still includes the fourth-order hyperdiffusion, which attenuates short horizontal wavelengths, and the effects of compressibility. In this section, we present an even simpler linear and incompressible model. Because the model is linear, the fourth-order hyperdiffusion used to guarantee the stability of the integration in the nonlinear model is not necessary.

a. Model equations

The linear simulation was performed by integrating the linearized, two-dimensional Bousinesq equations:

$$\left(\frac{\partial}{\partial t} + \overline{U}(z)\frac{\partial}{\partial x}\right)u' + w\frac{d\overline{U}(z)}{\partial z} + \frac{1}{\rho_o}\frac{\partial p'}{\partial x} = 0 \quad (1)$$

$$\left(\frac{\partial}{\partial t} + \overline{U}(z)\frac{\partial}{\partial x}\right)w' + \frac{1}{\rho_o}\frac{\partial p'}{\partial z} = b \quad (2)$$

$$\left(\frac{\partial}{\partial t} + \overline{U}(z)\frac{\partial}{\partial x}\right)b + w'N^2(z) = Q_l(x,z,t) \quad (3)$$

$$\frac{\partial u'}{\partial x} + \frac{\partial w'}{\partial z} = 0, \quad (4)$$

where $Q_l(x, z, t)$ represents the thermal forcing; u' is the perturbation horizontal wind; w' is the perturbation vertical velocity; b is the buoyancy, given by $g[\theta'/\overline{\theta}(z)]$, where θ' is the perturbation potential temperature; $\overline{\theta}(z)$ is the mean potential temperature; and g is the acceleration due to gravity. Here $N(z)$ is also defined in terms of potential temperature as $N^2 = (g/\overline{\theta})(\partial\overline{\theta}/\partial z)$. Both the mean wind $\overline{U}(z)$ and the buoyancy frequency $N(z)$ can vary in the vertical. The vertical momentum equation [(2)] includes nonhydrostatic terms, $[(\partial/\partial t) + \overline{U}(z)(\partial/\partial x)]w'$, since the spectra of the stratospheric gravity waves in the nonlinear and quasi-linear simulations included a significant amount of energy in the nonhydrostatic regime.

The numerical integration of (1)–(4) is described in appendix A of Pandya et al. (1996). Analytic solutions of these equations have been used in other studies (e.g. Lin and Smith 1986; Bretherton 1988; Nicholls et al. 1991; Pandya et al. 1993), but these analytic techniques have two principal disadvantages for our purpose: they are useful only in vertically uniform mean states, which are not representative of real world convection; and they are based on the further assumption that the solutions are hydrostatic, which is not true for a significant fraction of the stratospheric gravity waves above deep convection. The numerical integration of (1)–(4) incorporates an upper boundary condition similar to that in Klemp and Durran (1983), which allows only upwardly propagating waves. Open lateral boundaries are approximated by using a periodic horizontal domain much larger than the horizontal scale of the perturbed flow.

The numerical integration of (1)–(4) does not parameterize subgrid-scale processes like Richardson number–dependent eddy mixing. While this represents a conceptual simplification, it ignores a potentially important physical process, particularly for small vertical and horizontal wavelength features. Further, the linear model does not utilize any artificial smoothing (hyperdiffusion) of the kind necessary to ensure stability in the nonlinear model used for the simulation presented in AHD as well as the quasi-linear simulation.

The linear simulation was performed in a domain 2250 km in the horizontal and 32 km in the vertical. The horizontal grid spacing was $\Delta x = 1500$ m, the vertical grid spacing was $\Delta z = 250$ m, and a 6-s time step was used. Of the 2250 km long computational domain, only the central 840 km was used for analysis of the stratospheric gravity waves. The depth of the domain, the horizontal resolution, and the time step were all chosen to match the nonlinear and quasi-linear simulations.

b. Thermal forcing

Thermal forcing $Q_l(x, z, t)$ is derived from the pattern of latent heating and cooling produced by microphysics in the nonlinear squall line simulation of AHD in the same way as for the quasi-linear simulation. The thermal forcing in the linear model, $Q_l(x, z, t)$, is actually a forcing for the buoyancy [see Eq. (3)] and has units of meters per second cubed. The latent heating and cooling in the nonlinear model is the potential temperature tendency produced by microphysical processes and has units of kelvins per second. The linear buoyancy forcing is related to the nonlinear diagnosed latent heating and cooling by

$$\hat{Q}_l(x, p, t) = \frac{g}{\overline{\theta}(p)}\hat{Q}_{nl}(x, p, t).$$

Applying the diagnosed heating and cooling from the nonlinear squall line simulation to the linear model was complicated by the fact that the linear model was incompressible while the nonlinear model was compressible. In the compressible atmosphere of the nonlinear simulation the variation of density with height results in an exponential decrease in the pressure with height. In the linear incompressible model, density is assumed constant, and the pressure varies linearly with height. Thus, it is impossible to preserve the thermal forcing's functional dependence on z and p simultaneously. Since pressure is the dynamical variable, we chose to preserve the functional dependence of the heating on the pressure. To find $Q_l(x, z, t)$ from $\hat{Q}_{nl}(x, p, t)$ a hydrostatic mean state with a constant density of 0.7 kg m^{-3} is assumed for the linear model. This density is the average tropospheric value of the density in the nonlinear model. From this an initial $p(z)$ can be calculated in the linear model, and $Q_l(x, z, t)$ is computed by linear interpolation of $\hat{Q}_l(x, p, t)$. The interpolation is only necessary in the troposphere, since the thermal forcing in the nonlinear model never extended above the tropopause. A snapshot of $Q_l(x, z, t)$, at 6 h is shown in Fig. 6a; the pattern of latent heating and cooling in the nonlinear model $Q_{nl}(x, z, t)$ at the same time is shown in Fig. 6b for comparison. Note that the units and contour intervals are different for the two figures.

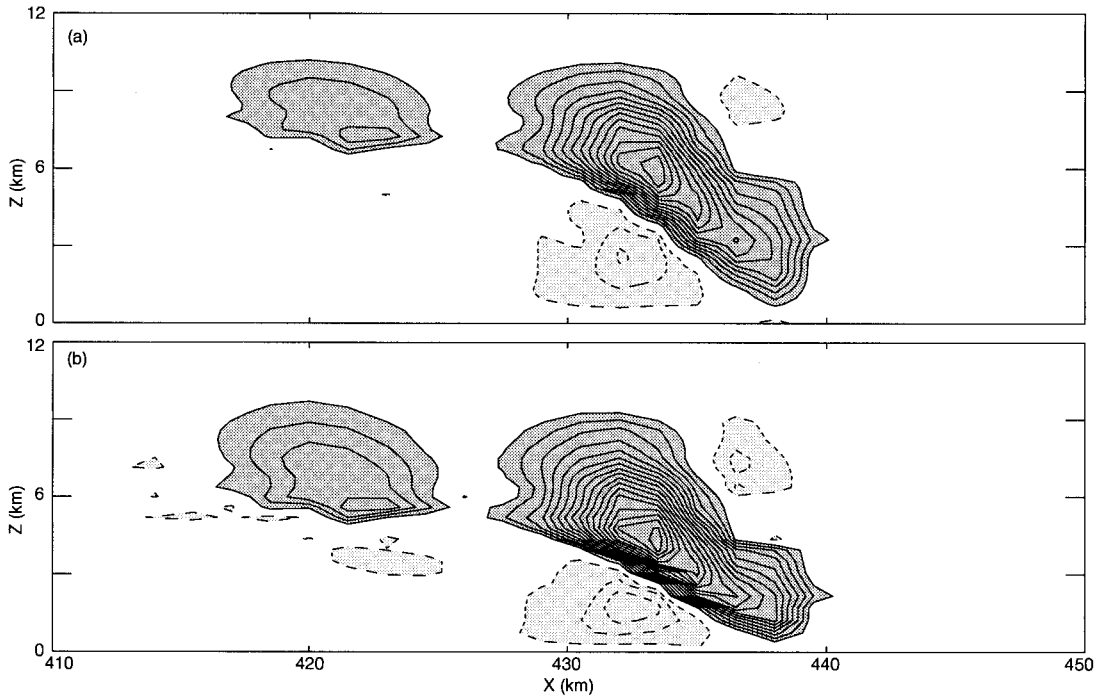

FIG. 6. (a) The specified pattern of thermal forcing in the linear model at 6 h; (b) the instantaneous pattern of latent heating and cooling in the nonlinear simulation at 6 h. Contour interval is (a) 0.002 m s^{-3} and (b) 0.005 K s^{-1}.

c. Initial conditions

The horizontally uniform mean wind and buoyancy frequency used in the linear simulation are shown in Figs. 7a and 7b, respectively. These initial conditions are meant to match the initial conditions in the nonlinear and quasi-linear simulations. As with the thermal forcing, however, the incompressibility of the linear model made it impossible to simultaneously match the height and pressure dependence of the initial conditions in both models. We chose to preserve the pressure dependence in order to be consistent with the thermal forcing. In the troposphere, the mean wind and buoyancy frequency were determined in the same manner as the thermal forcing: by using linear interpolation and assuming that the pressure is in hydrostatic balance and that the density is a constant 0.7 kg m^{-3}. In the stratosphere, values of the mean wind and buoyancy frequency do not change with height or pressure, so no interpolation is necessary. The mean winds and buoyancy frequency are shown with the solid lines in Fig. 7 and can be compared to the initial winds and buoyancy frequency of the nonlinear and quasi-linear simulations, which are shown in Figs. 1a and 1b of AHD. This comparison reveals that preserving the pressure dependence of the winds and buoyancy has the strongest effect at low-levels and relatively little effect at middle and upper levels. The dotted line in Fig. 7b shows a second buoyancy frequency profile, which will be discussed in section 6.

5. Linear simulation

Figure 8a shows the vertical velocity that develops in the linear simulation. Comparing this to the nonlinear and quasi-linear simulations, shown in Fig. 1, reveals that the linear simulation has significantly higher amplitude in the stratospheric waves than either the nonlinear or quasi-linear simulations. (Care should be taken in this comparison since the contours shown are not the same in these figures.) As in the other simulations, however, the linear simulation produces many more westward-propagating waves than eastward-propagating waves. The fanlike structure of the waves to the west of the tropospheric updraft at $x = 450$ km is visible in the linear simulations for $x > 400$ km. For $x < 400$ km, however, the fanlike wave pattern is not visible. Instead, the linear vertical velocity field is dominated by short horizontal wavelength waves not present in the nonlinear simulation.

Figure 9 shows the power spectra (thick black lines) in the linear simulation. Figure 9 also shows the nonlinear (thick gray lines) and quasi-linear (thin gray lines) spectra for comparison. The spectra for all the linear simulations are computed in the same way as in the nonlinear and quasi-linear simulations except that the vertical velocity in the linear simulations was not scaled with height as in the nonlinear and quasi-linear simulations. Since the linear model is incompressible, the amplitude of the waves does not grow with height, which renders the scaling unnecessary.

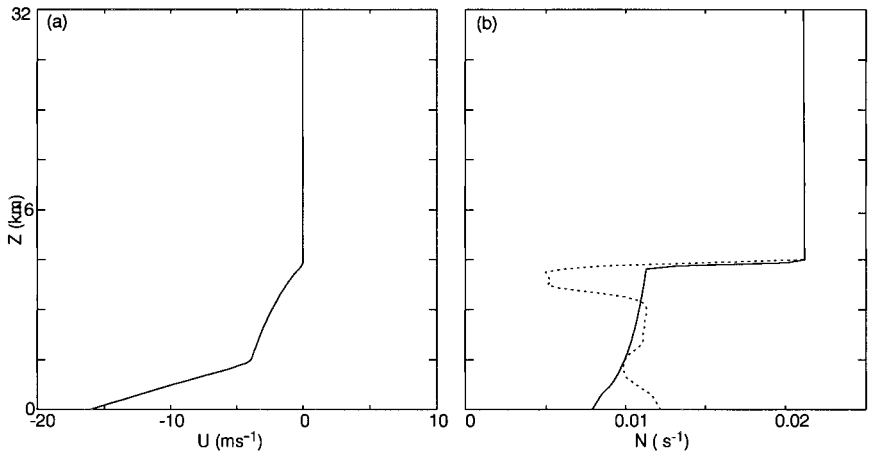

FIG. 7. The (a) mean wind and (b) buoyancy frequency (solid line) in the linear simulation. (b) The dotted line is the buoyancy frequency profile that includes the region of reduced stability near the tropopause discussed in section 6.

Comparing the horizontal wavenumber spectra shown in Fig. 9a reveals that the linear spectra and the quasi-linear spectra agree for horizontal waves longer than ~20 km. The spectra in the quasi-linear and nonlinear simulations fall off sharply for waves with a horizontal wavelength of less than ~10 km. AHD attributed the precipitous drop of the nonlinear spectrum at short horizontal wavelengths to the fourth-order hyperdiffusion used in the nonlinear model in order to maintain numerical stability. This artificial hyperdiffusion was also used in the quasi-linear simulation and accounts for the rapid falloff at short horizontal wavelengths in the quasi-linear spectrum. Since linear simulations do not require smoothing to preserve stability, we did not use any hyperdiffusion; thus, the linear simulation produces significantly more short horizontal waves than the nonlinear simulation. Some of these waves are visible in the vertical velocity shown in Fig. 8 as the packet of short horizontal wavelength waves between $z = 16$ km and $z = 24$ km and between $x = 380$ km and $x = 300$ km. The thin dark line in Fig. 9 shows the effect of a simple fourth-order filter (k^{-4}) applied to the spectra from the linear model. This fourth-order filter is meant to be equivalent to the fourth-order hyperdiffusion in the nonlinear and quasi-linear simulations. With the fourth-order filter, the power spectrum in the linear model drops off steeply at short wavelengths and more closely resembles the quasi-linear spectrum, suggesting that the principal difference between the quasi-linear and linear simulations is a result of the artificial fourth-order hyperdiffusion in the quasi-linear simulation.

The vertical wavenumber and frequency spectra, shown in Figs. 9b and 9c, respectively, are qualitatively similar to the quasi-linear spectra, although the power in the linear spectra is uniformly larger than the power in the quasi-linear spectra. This difference, however, is primarily the result of the short horizontal wavelength modes that are removed from the quasi-linear simulation by the artificial fourth-order hyperdiffusion. Both the vertical wavelength and frequency spectra for the linear

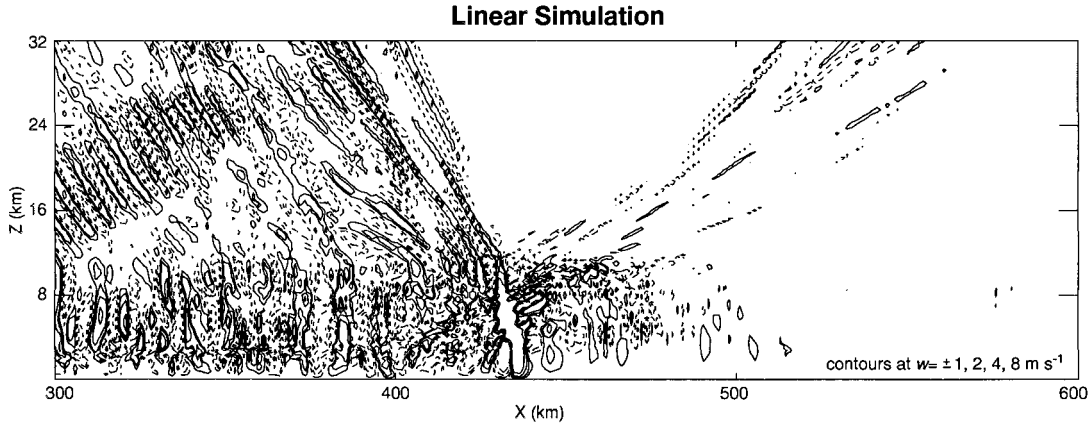

FIG. 8. Vertical velocity 6 h into the linear simulation. Contours at ±1, 2, 4, and 8 m s^{-1}; negative contours dashed.

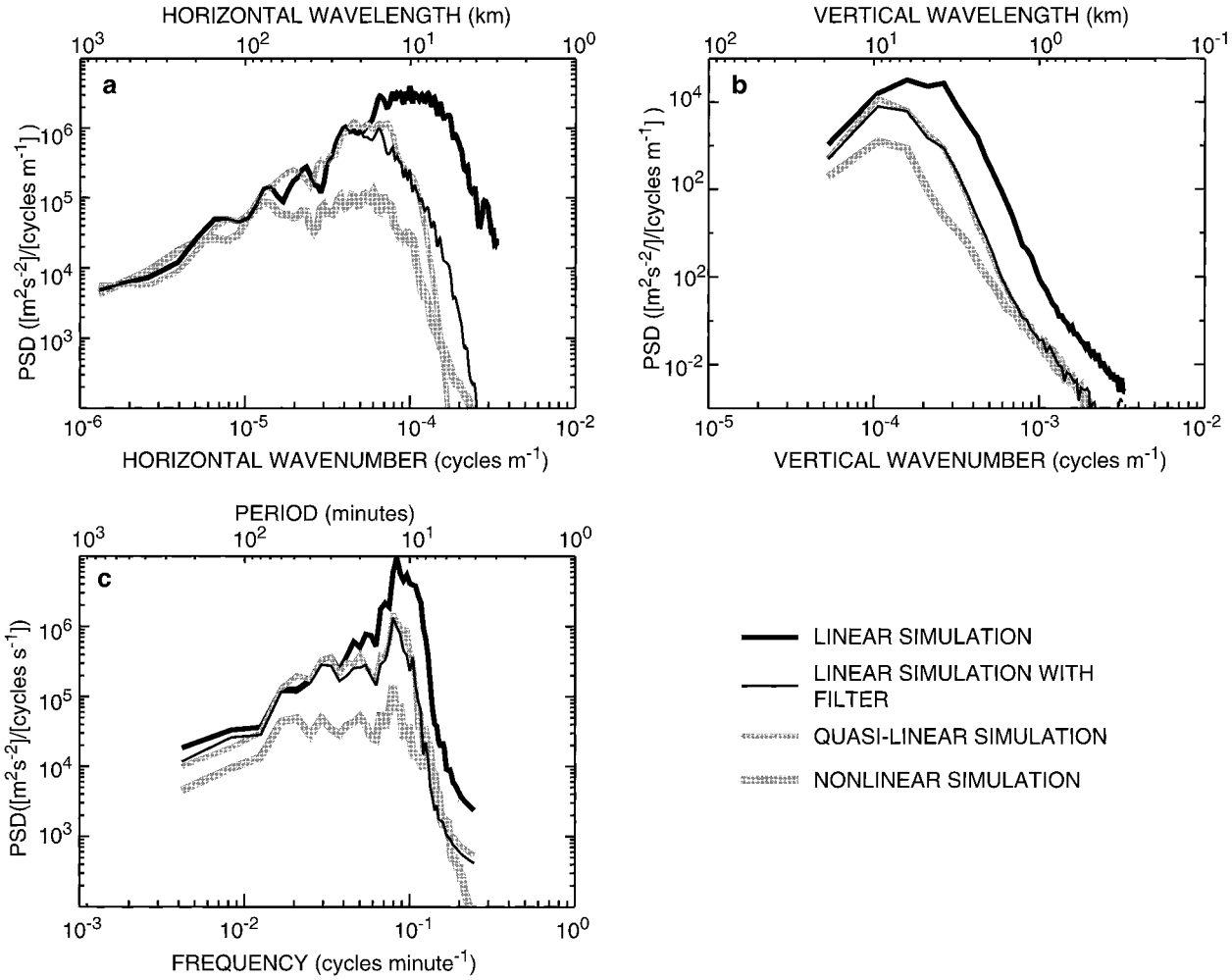

FIG. 9. Power spectra of the stratospheric vertical velocity for the linear simulation (thick black line) and linear simulation with a fourth-order horizontal wavenumber filter (thin black line) as a function of (a) horizontal wavenumber, (b) vertical wavenumber, and (c) frequency. For comparison, the lightly shaded gray lines show the spectra in the quasi-linear (thin) and nonlinear (thick) simulations. (c) The hatched bar marks the dominant period of 12 min.

simulation with the application of a fourth-order filter in horizontal wavenumber (given by the thin black line) agree almost perfectly with the quasi-linear spectra.

6. Linear simulation with a low-stability layer

The results of the previous section raise the question of whether the artificial hyperdiffusion in the nonlinear model is removing an important part of the spectra by removing the short-wavelength waves. We performed an additional simulation to address this question. In this additional simulation, a region of low stability is inserted below the troposphere. This region of low-stability represents the change in the stability that forms around real storms (see Fig. 1 of AHD).

The modified stability profile is shown as the dotted line in Fig. 7b. This stability profile was computed by averaging the stability profiles in the 200-km horizontal region centered around the storm's leading edge from time 4–5 h in the nonlinear simulation. In moisture-saturated regions the conventional formula for the Brunt–Väisälä frequency was modified to take into account the effects of latent heat release on the static stability (Durran and Klemp 1982). We chose to average over 200 km to cover the main region where waves are generated.

Figure 10 shows the vertical velocity at time 6 h in the linear simulation with a low-stability layer. Comparing this to the vertical velocity field in the linear simulation, shown in Fig. 8, reveals that the low-stability layer significantly reduces the amplitude of the waves in the stratosphere while increasing the amplitude of the waves in the lower troposphere. Notice that the short horizontal wavelength packet in the linear simulation between $z = 16$ km and $z = 24$ km and between $x = 380$ km and $x = 300$ km in Fig. 10 is not present in the linear simulation with the low-stability layer.

Figure 11 compares the horizontal wavenumber spec-

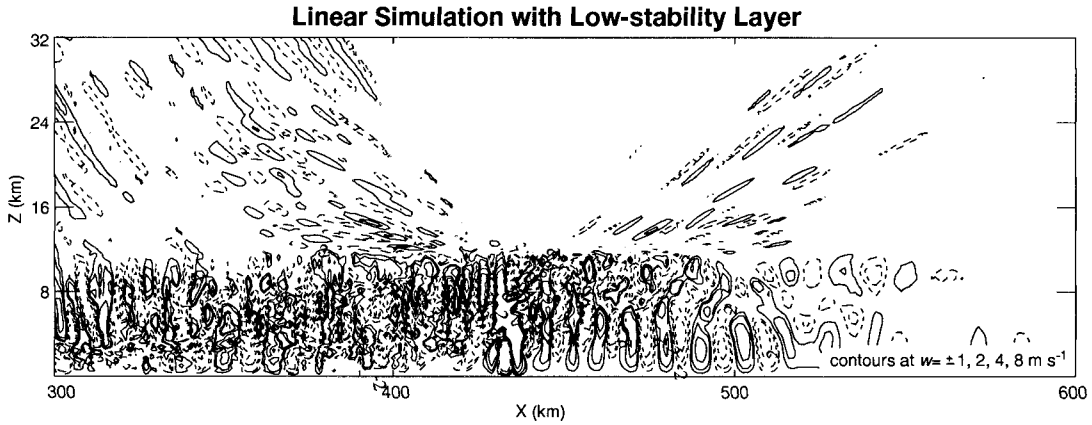

FIG. 10. Vertical velocity 6 h into the linear simulation with a modified stability layer. Contours at ± 1, 2, 4, and 8 m s^{-1}; negative contours dashed.

tra of the stratospheric waves in the linear simulations with (thin lines) and without (thick lines) the low-stability layer and confirms that the low-stability layer acts to remove small horizontal wavelength waves. This suggests that the inability of the nonlinear model to deal effectively with the smallest horizontal wavelengths is not problematic since these waves would be eliminated from the stratospheric wave spectra by the upper-tropospheric low-stability layer associated with the stratiform anvil.

We can understand how a low-stability layer acts to limit the amplitude of the power spectrum at shorter wavelengths by comparing the propagation of linear gravity waves through the two idealized atmospheres illustrated in Fig. 12. In the first case the atmosphere consists of two semi-infinite layers, each with constant stability and zero mean wind. The stability of the upper layer is N_2 and the lower layer is N_1, where $N_2 > N_1$. Thus, the upper layer corresponds to the stratosphere and the lower layer to the troposphere. Our analysis follows that of Crook (1988); we refer the reader to this source for a more detailed discussion of partial reflection. A monochromatic, linear gravity wave with vertical velocity given by $w = w_0 \exp[kx - m_1(z - H) - \omega t]$ is incident on the boundary between the two layers, which is assumed to be at height H. This wave is partially reflected, giving the downward-propagating wave $r_1 \exp[kx + m_1(z - H) - \omega t]$, and partially transmitted, giving the stratospheric, upward-propagating wave $t_2 \exp[kx - m_2(z - H) - \omega t]$. Neither the horizontal wavenumber k nor the frequency ω change in the reflected and transmitted waves. The vertical wavelength in the transmitted wave, however, changes as a result of refraction at the tropopause. The vertical wavelength in the stratosphere can be computed from the dispersion relation for hydrostatic gravity waves and can be either real (for propagating waves) or evanescent (for decaying waves). Once the vertical wavelength in the stratosphere is known, the amplitude of the transmitted wave t_2 as a fraction of the incident wave energy w_0 can be computed by matching w and $\partial w/\partial z$ at the tropopause.

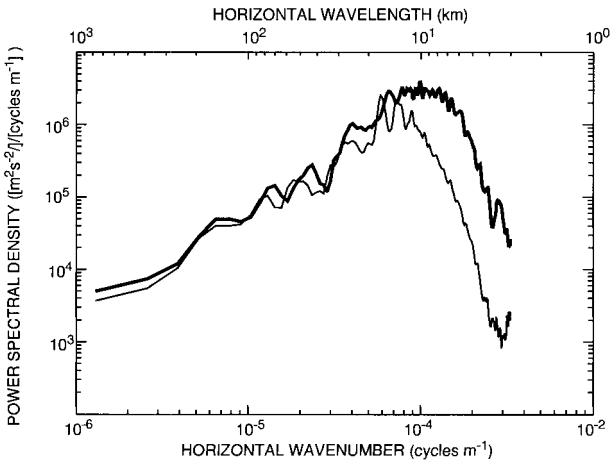

FIG. 11. Power spectra of the stratospheric vertical velocity as a function of horizontal wavenumber for the linear simulation with a low-stability layer (thin line) and the linear simulation (thick line).

We performed similar calculations for a three-layer atmosphere, which included a low-stability layer, with stability N_{low} and depth D, just below the tropopause. As before, we consider an upwardly propagating wave in the lowest layer given by $w = w_0 \exp[kx - m_1(z - H) - \omega t]$. Using the dispersion relation for hydrostatic gravity waves we can find the vertical wavelengths of the transmitted waves in the other two layers. Applying the continuity of vertical velocity and its first derivative at the interfaces at $z = H$ and $z = H - D$ allows us to solve for the amplitude of the upwardly propagating stratospheric gravity wave as a fraction of the incident wave energy. Thus, we can compare the fraction of the incident amplitude that is transmitted to the stratosphere in the two cases.

Figure 13 shows such a comparison for the idealized cases that correspond to the linear simulation and the

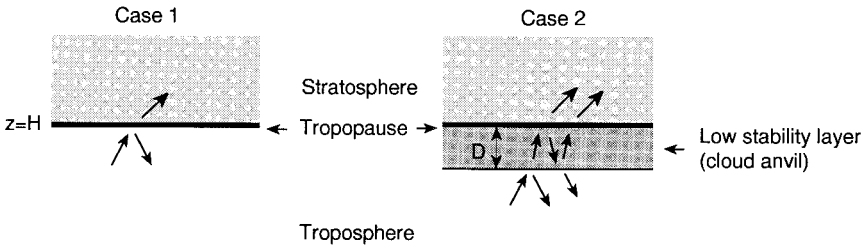

FIG. 12. Two idealized atmospheres used to investigate the upward propagation of gravity waves with and without a layer of reduced stability.

linear simulation with the modified buoyancy frequency. For this case, $N_1 = 0.02\ s^{-1}$, $N_2 = 0.01\ s^{-1}$, $N_{low} = 0.005\ s^{-1}$, the tropopause is at $H = 11$ km, and the low-stability layer has a depth, D, of 2 km. The ratio of amplitudes are computed for each combination of ω and k and then summed in ω to produce Fig. 13. The square of the amplitude is used rather than the amplitude in order to facilitate comparison with the power spectra, which are based on the wave amplitude squared. Note that the amplitude of the incident wave is assumed to be independent of the wavelength. Figure 13, then, shows how a low-stability layer would alter the power as a function of horizontal wavelength. It reveals that short horizontal wavelength modes will be most attenuated by the low-stability layer, while longer horizontal wavelength modes will pass through the low-stability layer largely unaffected. This agrees with the comparison of the spectra in the linear simulations with and without a reduced stability layer, which suggested that the low-stability layer primarily affects the shortest wavelengths. Thus, linear theory applied to a simplified structure involving only step changes in stability and ignoring the mean wind is sufficient to understand the qualitative effect of a layer of low stability on upwardly propagating gravity waves.

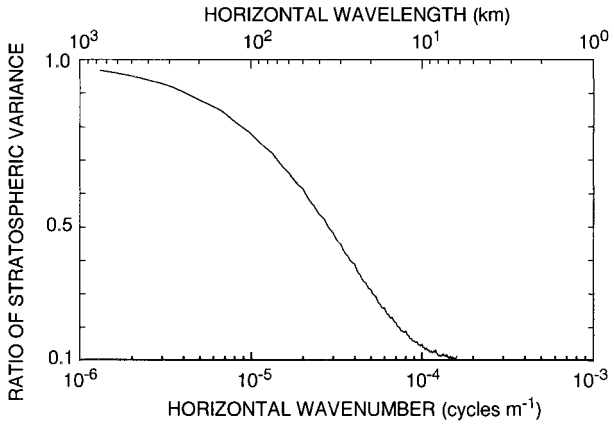

FIG. 13. Ratio of stratospheric wave amplitude squared in the idealized three-layer atmosphere to the stratospheric wave amplitude squared in the idealized two-layer atmosphere as a function of horizontal wavenumber.

7. Summary and conclusions

We conclude by comparing the spectra of gravity waves generated by a time- and space-varying thermal forcing in the linear, Bousinesq model to the spectra of gravity waves above organized convection in the nonlinear squall line simulation. Such a comparison reveals the extent to which linear dynamics can explain the gravity waves generated by organized convection. These spectra are shown in Fig. 9 of section 5, but are reproduced here in Fig. 14 for convenience.

The horizontal wavenumber spectra in both the linear and nonlinear model were broad and had no distinct peaks (see Fig. 14a). The amplitudes of the linear waves were significantly greater than the amplitudes of the nonlinear waves for horizontal wavelengths less than 100 km. For horizontal wavelengths less than 10 km, the nonlinear spectrum was severely attenuated by the fourth-order hyperdiffusion that was used to ensure stability in the nonlinear model. In real storms, the development of an extensive stratiform anvil produces a low-stability layer that prevents transmission of these shortest wavelengths into the stratosphere. Thus, the attenuation of small horizontal wavelengths by the hyperdiffusion in the nonlinear simulation is not physically significant since these waves would not propagate through the low stability in the trailing anvil anyway. The disagreement of the nonlinear and linear spectra for horizontal wavelengths between 10 and 100 km is, however, physically significant and may be related to the mixing processes active in the nonlinear simulation. In the nonlinear model, there is a Richardson number–dependent mixing parameterization that acts to redistribute horizontal momentum (Lilly 1962); this mixing was active in the troposphere within the stratiform cloud and extended over a horizontal region of ~100 km. Mixing could also affect the generation of gravity waves by convection though the spatial redistribution of the temperature perturbations in the convective region. In the linear model, there is no mixing and only the latent heating and cooling (and not the redistribution of sensible heat) associated with the convection is included in the thermal forcing.

The vertical wavenumber spectra of stratospheric vertical velocity in both the linear and nonlinear simula-

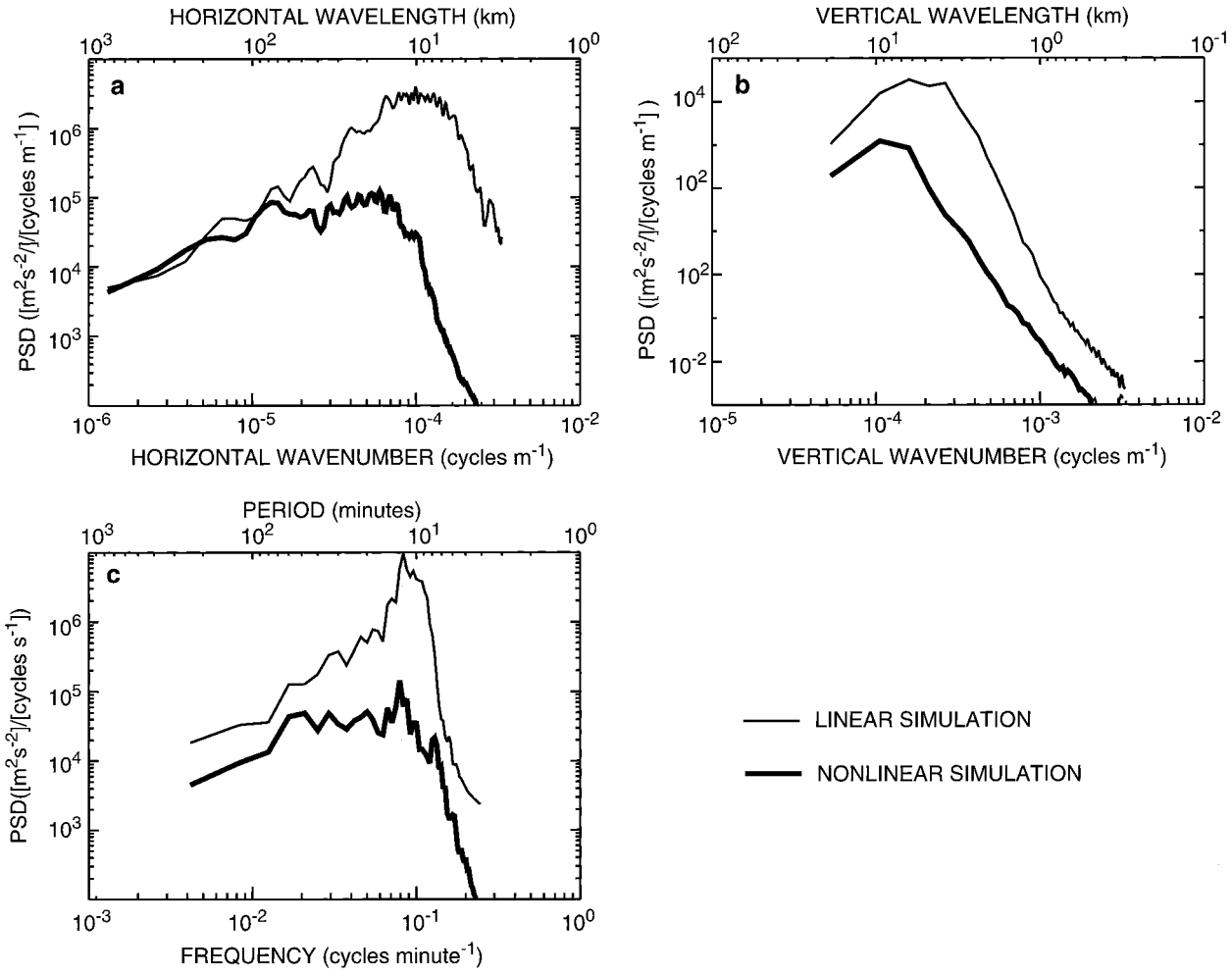

FIG. 14. Power spectra of the stratospheric vertical velocity for the linear simulation (thin line) and nonlinear simulation (thick line) as a function of (a) horizontal wavenumber, (b) vertical wavenumber, and (c) frequency. (c) The hatched bar marks the dominant period of 12 min.

tions are dominated by waves with a vertical wavelength of 6–10 km (see Fig. 14b). This dominant wavelength is determined by two things: the depth of the convective heating and the factor of 2 increase in stability at the tropopause. The heating in the troposphere has a half-sinusoidal structure and so projects most directly on modes with a vertical wavelength of twice the depth of the heating. As these modes travel across the tropopause, refraction decreases their vertical wavelength by the inverse in the stability jump across the tropopause. Typically, the stratospheric stability is twice that of the troposphere, which gives a factor of 2 increase in the wavelength and results in stratospheric vertical wavelengths equal to the depth of the heating. Since both refraction at the tropopause and projection onto modes with the same depth as the heating in the troposphere are linear processes, the vertical wavelength peak is captured in the linear simulations.

The frequency spectrum of the stratospheric vertical velocity shows a peak at ~12 min in both the linear and nonlinear simulations (see Fig. 14c). This peak is also evident in the dominant 64° tilt of the phase lines for the stratospheric waves. The frequency spectrum of the thermal forcing applied in the linear simulation also shows a peak at ~12 min, which corresponds to the period of convective cell formation in the nonlinear model. This periodicity in the forcing in the linear model leads to periodic tropospheric updrafts and downdrafts and pressure perturbations that excite waves in the stratosphere via the mechanical oscillator mechanism of Fovell et al. (1992).

In summary, linear theory seems to be able to capture the general characteristics of the gravity wave spectra above convection including the location of the peaks in the vertical wavelength and frequency spectrum. We have also shown that linear theory fails to predict the correct amplitude of the wave response due to nonlinear processes that affect waves with a horizontal wavelength between 10 and 100 km.

These results suggest two observationally testable hy-

potheses: that the dominant vertical wavelengths in the stratosphere should correspond to the depth of the convective cloud in the troposphere and the frequencies of the stratospheric waves should correspond to the periodicities in the tropospheric convective heating. These results can also be used as the basis for developing a parameterization of convectively generated gravity waves for larger-scale models like GCMs. One can imagine using large-scale variables to predict the height of convection, and therefore the dominant vertical wavelength. Large-scale variables such as the amount and location of wind shear may influence the periodicity of convection (Weisman et al. 1988; Fovell and Dailey 1995), which would allow one to predict the dominant frequency of the stratospheric waves. The amplitude of the stratospheric waves would be more difficult to determine since the linear relationships between convection and stratospheric waves does not extend to amplitude.

Acknowledgments. This work was supported by NASA Grant NAG-1-1803 and the Physical Meteorology Program of the National Science Foundation Grant ATM-9525746. Support for REP comes from the Advanced Study Program at the National Center for Atmospheric Research. The authors would like to thank Dr. Michael McIntyre for originally suggesting this study, as well as Professor James Holton, Drs. R. Garcia and J. Klemp, and three anonymous reviewers for their comments that significantly improved the manuscript.

REFERENCES

Alexander, M. J., J. R. Holton, and D. R. Durran, 1995: The gravity wave response above deep convection in a squall line simulation. *J. Atmos. Sci.,* **52,** 2212–2226.

Andrews, D. G., J. R. Holton, and C. B. Leovy, 1987: *Middle Atmosphere Dynamics.* Academic Press, 489 pp.

Bergman, J. W., and M. L. Salby, 1994: Equatorial wave activity derived from fluctuations in observed convection. *J. Atmos. Sci.,* **51,** 3791–3806.

Bretherton, C., 1988: Group velocity and the linear response of stratified fluids to internal heat or mass sources. *J. Atmos. Sci.,* **45,** 81–93.

Crook, N. A., 1988: Trapping of low-level internal gravity waves. *J. Atmos. Sci.,* **45,** 1533–1541.

Dewan, E. M., and Coauthors, 1998: MSX satellite observations of thunderstorm-generated gravity waves in mid-wave infrared images of the upper stratosphere. *Geophys. Res. Lett.,* **25,** 939–942.

Durran, D. R., and J. B. Klemp, 1982: On the effects of moisture on the Brunt–Väisälä frequency. *J. Atmos. Sci.,* **39,** 2152–2158.

Edmon, H. J., Jr., B. J. Hoskins, and M. E. McIntyre, 1980: Eliassen–Palm cross sections for the troposphere. *J. Atmos. Sci.,* **37,** 2600–2616.

Fovell, R. G., and P. S. Dailey, 1995: The temporal behavior of numerically simulated multicell-type storms. Part I: Modes of behavior. *J. Atmos. Sci.,* **52,** 2073–2095.

——, D. R. Durran, and J. R. Holton, 1992: Numerical simulations of convectively generated stratospheric gravity waves. *J. Atmos. Sci.,* **49,** 1427–1442.

Gage, K. S., and B. B. Balsley, 1984: MST radar studies of wind and turbulence in the middle atmosphere. *J. Atmos. Terr. Phys.,* **46,** 739–753.

Garcia, R. R., and M. L. Salby, 1987: Transient response to localized episodic heating in the Tropics. Part II: Far-field behavior. *J. Atmos. Sci.,* **44,** 498–530.

Holton, J. R., 1973: On the frequency distribution of atmospheric Kelvin waves. *J. Atmos. Sci.,* **30,** 499–501.

——, 1992: *An Introduction to Dynamic Meteorology.* Academic Press, 507 pp.

Klemp, J. B., and D. R. Durran, 1983: An upper boundary condition permitting internal gravity wave radiation in numerical mesoscale models. *Mon. Wea. Rev.,* **111,** 430–444.

Larsen, M. F., W. E. Swartz, and R. F. Woodman, 1982: Gravity-wave generation by thunder storms observed with a vertically-pointing 430 MHz radar. *Geophys. Res. Lett.,* **9,** 571–574.

Lilly, D. K., 1962: On the numerical simulation of buoyant convection. *Tellus,* **14,** 148–172.

Lin, Y. L., and R. B. Smith, 1986: Transient dynamics of airflow near a local heat source. *J. Atmos. Sci.,* **43,** 40–49.

Manzini, E., and K. Hamilton, 1993: Middle atmosphere traveling waves forced by convective heating. *J. Atmos. Sci.,* **50,** 2180–2200.

Mapes, B. E., 1993: Gregarious tropical convection. *J. Atmos. Sci.,* **50,** 2026–2037.

Nicholls, M. E., R. A. Pielke Sr., and W. R. Cotton, 1991: Thermally forced gravity waves in an atmosphere at rest. *J. Atmos. Sci.,* **48,** 1869–1884.

Pandya, R. E., and D. R. Durran, 1996: The influence of convectively generated thermal forcing on the mesoscale circulation around squall lines. *J. Atmos. Sci.,* **53,** 2924–2951.

——, ——, and C. Bretherton, 1993: Comments on ''Thermally forced gravity waves in an atmosphere at rest.'' *J. Atmos. Sci.,* **50,** 4098–4101.

Percival, D. B., and A. T. Walden, 1993: *Spectral Analysis for Physical Applications*: *Multitaper and Conventional Univariate Techniques.* University Press, 702 pp.

Salby, M. L., and R. R. Garcia, 1987: Transient response to localized episodic heating in the Tropics. Part I: Excitation and short-time near-field behavior. *J. Atmos. Sci.,* **44,** 458–498.

Sato, K., 1993: Small-scale wind disturbances observed by the MU radar during the passage of Typhoon Kelly. *J. Atmos. Sci.,* **50,** 518–537.

Simpson, J., C. Kummerow, W.-K. Tao, and R. F. Adler, 1996: On the Tropical Rainfall Measuring Mission (TRMM). *Meteor. Atmos. Phys.,* **60,** 19–36.

Weisman, M. L., J. B. Klemp, and R. Rotunno, 1988: Structure and evolution of numerically simulated squall lines. *J. Atmos. Sci.,* **45,** 1990–2013.

Yang, M.-J., and R. A. Houze Jr., 1995: Multicell squall-line structure as a manifestation of vertically trapped gravity waves. *Mon. Wea. Rev.,* **123,** 641–661.